Astrodynamics Vol. 7, No. 4, 383–399, 2023 https://doi.org/10.1007/s42064-023-0159-3

# Design and guidance of a multi-active debris removal mission

**Minduli C. Wijayatunga[1](✉), Roberto Armellin[1], Harry Holt[1], Laura Pirovano[1], and Aleksander A. Lidtke[2]**

*1. Te Pūnaha Ātea – Space Institute, The University of Auckland, Auckland 1010, New Zealand*
*2. Astroscale Japan Inc., 1-16-4-16 Kinshi, Sumida-ku, Tokyo, Japan*

**ABSTRACT**

Space debris have become exceedingly dangerous over the years as the number of objects in orbit continues to increase. Active debris removal (ADR) missions have gained significant interest as effective means of mitigating the risk of collision between objects in space. This study focuses on developing a multi-ADR mission that utilizes controlled reentry and deorbiting. The mission comprises two spacecraft: a Servicer that brings debris to a low altitude and a Shepherd that rendezvous with the debris to later perform a controlled reentry. A preliminary mission design tool (PMDT) was developed to obtain time and fuel optimal trajectories for the proposed mission while considering the effect of $J_2$, drag, eclipses, and duty cycle. The PMDT can perform such trajectory optimizations for multi-debris missions with computational time under a minute. Three guidance schemes are also studied, taking the PMDT solution as a reference to validate the design methodology and provide guidance solutions to this complex mission profile.

**KEYWORDS**

active debris removal (ADR)
trajectory design optimization
autonomous guidance
low-thrust electric propulsion
$\Delta v$-law guidance
Q-law guidance

**Research Article**

Received: 12 October 2022
Accepted: 29 January 2023


## 1 Introduction

The space environment in the low Earth orbit (LEO) is becoming increasingly congested with space debris. As a result, the average rate of debris collisions has increased to four or five objects per year [1]. Most debris consist of artificial objects, such as derelict satellites, discarded rocket stages, and fragments originating from collisions. As satellites become increasingly essential to daily life, an increasing number of satellites are added to expand space-enabled services. However, additional launches increase the risk of collision for all satellites as they further saturate space with objects, thereby endangering critical space infrastructure. A collision in space can create debris that can collide with other space objects and generate more debris. This cascading effect is known as the "Kessler syndrome", named after D. J. Kessler [2, 3]. Kessler *et al.* [3] discussed the frequency of collisions and their consequences, describing standard mitigation techniques for the first time. Subsequently, Pelton [4] discussed the cascading effect of collisions and international standards for debris mitigation and space traffic management. He also provided estimates of the number of orbital debris at the time to be approximately six metric tons in mass and 22,000 in number. Several events in recent history have caused significant additions to the space debris population. These include the anti-satellite missile tests in 2007 and 2021, and the collision of Iridium 33 and Kosmos 2251 in 2009 [5, 6].

Active debris removal (ADR) is the process of removing derelict objects from space, thus minimizing the build-up of unnecessary objects and lowering the probability of on-orbit collisions that can fuel a "collision cascade" [7, 8]. ADR has become significant over the past two decades, leading to numerous studies and implementations of potential debris removal missions and technologies. The ELSA-d mission designed by Astroscale was launched in March 2021 and has successfully tested both rendezvous algorithms required for ADR and a magnetic capture mechanism to remove objects carrying a dedicated

✉ mwij516@aucklanduni.ac.nz

**Nomenclature**

| | | | |
|---|---|---|---|
| ADR | active debris removal | PMDT | preliminary mission design tool |
| DC | duty cycle | RAAN | right ascension of the ascending node |
| LEO | low Earth orbit | TOF | time of flight |

docking plate at the end of their missions[①]. The RemoveDebris mission by the University of Surrey is another project that demonstrated various debris removal methods, including harpoon and net capture [9]. The CleanSpace-1 mission by the European Space Agency (ESA) aims to deorbit a 112 kg upper stage of a Vega rocket[②].

While individual removals are essential milestones towards ADR implementation, a deployment on a larger scale, targeting more objects, might be necessary [8, 10]. To make this financially feasible, each ADR Servicer might require to remove more than one object and use mass-efficient low-thrust electric propulsion (EP). This combination of long, EP-based transfers and complex vehicle paths rendezvousing with multiple moving targets presents a difficult optimization challenge that must be addressed at the design stage of ADR missions. Because of the large number of potential ADR targets to be visited, transfers between consecutive mission orbits must be analyzed quickly to enable design iteration and parametric studies.

This paper introduces a novel multi-ADR removal mission concept that involves a two-spacecraft system. By request, the system would provide contact-based debris removal through a rendezvous and deorbit process. One spacecraft, called the Servicer, is reused for multiple pieces of debris, enabling the mission costs to remain low. The other spacecraft, the Shepherd, performs coupled reentry with the debris; therefore, the reentry process can be controlled adequately, thus complying with the ground-casualty risk requirements. The majority of the mission utilizes EP. This paper discusses the proposed mission in detail and develops a mission design tool to simulate multi-ADR tours accurately and efficiently.

To this end, a preliminary mission design tool (PMDT) is developed to optimize both the fuel consumption and time of flight (TOF) of multi-target missions while considering the effect of $J_2$, eclipses, and duty cycle. The PMDT exploits $J_2$ to achieve right ascension of ascending node (RAAN) changes to reduce the fuel consumption of the mission.

The PMDT extends the traditional Edelbaum method by introducing the contribution of drag and duty cycle. Phasing orbits are used for matching RAAN when required, as discussed in Ref. [11]. Finally, the altitude and inclination of the phasing orbits are optimized to obtain either time- or fuel-optimal trajectories. The sequence of targets can also be treated as an optimization variable in the PMDT. However, it was treated as a constant in the examples given in this study.

Our approach shares similarities with the Multidisciplinary desigN Electric Tug tool (MAGNETO) developed in Ref. [12] as well as the work by Viavattene *et al.* in Ref. [13]. However, it develops the presented models further by considering duty cycles and a more accurate description of eclipses and drag. Furthermore, the tool considers mission-specific constraints and uses an optimizer to perform rapid design iterations and parametric studies of the proposed multi-ADR mission.

Three guidance laws are used to assess the accuracy of the models adopted in the PMDT. Ruggiero *et al.* [14] developed a series of closed-loop guidance laws based on the Gauss form of Lagrange planetary laws. Locoche [15] developed a guidance law based on Lyapunov feedback control known as the $\Delta v$-law to supplement preliminary mission design tools. Finally, Petropoulos [16] developed one of the most versatile and well-known control laws, the Q-law, which is also based on Lyapunov control. These three approaches are used here to optimally track the transfers computed by the PMDT, thus validating its key assumptions and providing a possible approach for flying the missions.

The remainder of this paper is organized as follows. First, the mission concept of operations is presented. Then, the design of the PMDT is discussed and used to generate optimal debris removal trajectories at high computational speeds. Third, guidance schemes implemented on the PMDT outcomes are discussed.

① https://astroscale.com/astroscales-elsa-d-mission-successfully-completes-complex-rendezvous-operation/
② https://www.esa.int/Space_Safety/ClearSpace-1

The results section provides an example trajectory optimization solution for both a time- and mass-optimal multi-ADR mission. Finally, the paper's outcomes are summarized, and conclusions are drawn regarding the method's usefulness.

## 2 Concept of operations of the multi-ADR mission

The proposed multi-ADR mission architecture is shown in Fig. 1, where two spacecraft are involved in the debris removal process. A Servicer is used to approach and rendezvous with the debris. When the rendezvous is achieved, the Servicer brings the object to a low altitude orbit ($\approx$ 350 km in this study). The debris is then handed over to a Reentry Shepherd, which docks with the debris and performs a controlled reentry on its behalf. Controlled reentry reduces the casualty risk posed by removing the debris, which is desirable because the ADR targets are, by definition, large and thus contain components likely to survive the reentry. The Servicer can be reused for several debris removals, while each Reentry Shepherd can only be used once as it burns while deorbiting the debris. A handover altitude of 350 km was selected to reduce the $\Delta v$ required of the Servicer by minimizing the orbital transfers it requires to perform while ensuring the technical feasibility of the Shepherd and satisfying safety constraints posed by the altitude of the International Space Station (ISS).

The proposed mission architecture can perform multi-ADR services significantly cheaper than using a monolithic spacecraft, which would perform all the mission phases and then burn in the atmosphere after removing a single debris [17]. This is because the development and operation costs of a space mission are proportional to the system's dry mass [18]. Thus, although launching one Servicer and $n$ Shepherds to remove $n$ debris requires one more launch than using $n$ monolithic spacecraft, it is expected to be cheaper because of the lower overall mass that must be launched. This mass, and therefore also cost, saving provided by launching specialized spacecraft is further enhanced by the fact that the two spacecraft can be made smaller than a single monolithic spacecraft. Note that the Servicer proposed here is not obligated to carry re-entry-related hardware, thus saving dry mass and fuel. In addition, the Shepherd is not required to perform extensive orbital changes or have a long lifetime in space, thus reducing its size. These smaller spacecraft might be launched on cheaper dedicated rockets, further reducing the costs and offsetting the added complexity of operating two spacecraft instead of one. Furthermore, depending on the debris characteristics and governing regulations, the requirements of controlled reentry for each piece of debris will differ. The use of the Reentry Shepherd provides flexibility in performing controlled reentry of large-scale objects.

Trajectory optimization for this mission through traditional methods is non-intuitive, as multiple transfer arcs and targets are involved. Hence, in Section 3, a trajectory optimization tool that can develop suboptimal solutions with limited computational effort is described.

## 3 Methodology

### 3.1 Design of the preliminary mission design tool

In the 1960s, an analytical solution for the transfer between two inclined circular orbits under continuous thrust was developed by Theodore N. Edelbaum [19]. While the transfer arcs developed were both time- and fuel-optimal, they were obtained under the assumption of continuous thrust and the lack of other perturbations

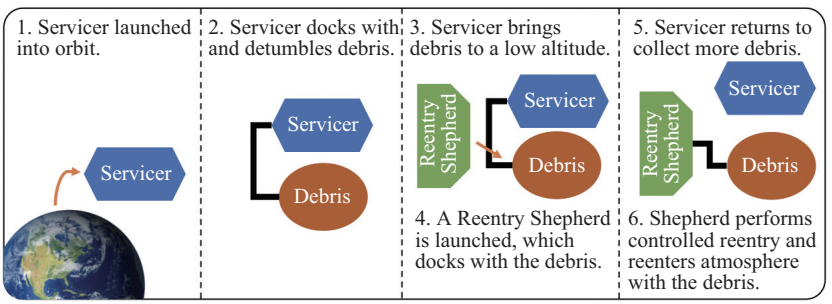


**Fig. 1** Mission architecture of the multi-ADR mission.

such as $J_2$ and air resistance. Several studies were conducted following Edelbaum's work to include the effect of discontinuous thrust and orbital perturbations on the problem dynamics. Colasurdo and Casalino [20] extended Edelbaum's analysis to compute optimal quasi-circular transfers while considering the effect of the Earth's shadow, and Kechichian [21] developed a method of calculating coplanar orbit-raising maneuvers considering eclipses while constraining the eccentricity to zero. However, both Refs. [20, 21] could only provide suboptimal solutions as they utilized thrust steering to maintain zero eccentricity. In 2011, Kluever [22] further extended Kechichian's method into a semi-analytic method that considers the effect of $J_2$ and Earth-shadow arcs. This method used Edelbaum-based orbital elements to compute the Earth-shadow arc during the transfer. However, it failed to consider the effect of air resistance, which is crucial for LEO transfers. In 2019, Cerf [11] proposed the use of $J_2$ to achieve RAAN changes during transfers to reduce fuel consumption while maintaining the TOF. However, they did not consider the effects of eclipses and air resistance. The PMDT is developed to unite the concepts given in Refs. [11, 19, 22] and develop them further by considering air resistance and duty cycle.

The PMDT first calculates the TOF and fuel expenditure of a single transfer using Edelbaum's method described in Ref. [19]. Then, additions to the classical Edelbaum method, such as creating the extended Edelbaum method (Algorithm 1), are performed to consider the effect of atmospheric drag, engine duty cycle, and solar eclipses. Third, an RAAN matching algorithm (Algorithm 2) that does not utilize fuel to perform RAAN adjustments is implemented to make transfers cheaper. This is achieved by introducing an intermediate phasing orbit in which the Servicer can utilize the effect of $J_2$ perturbations to reach the desired RAAN. Finally, this process is introduced into an optimization scheme (Fig. 3) in which the launch time and phasing orbits involved can be optimized to achieve the minimum TOF or minimum fuel expenditure.

### *3.1.1 Extended Edelbaum method*

The extended Edelbaum method is a version of the classical Edelbaum method adapted to consider the effect of atmospheric drag, solar eclipses, and duty cycles. This method is detailed in Algorithm 1. Note that this method can only ensure that a desired semi-major axis and inclination are reached.

To consider the effect of drag, the drag acceleration is calculated at the current node. Then, the semi-major axis variation due to drag at the next node is calculated, and the semi-major axis value of that node is updated to include the decrement due to drag.

A weighting factor equal to the fraction of eclipse time per orbit is obtained to account for eclipses. This is performed by sampling the current orbit at several points for one orbital period and observing how many of those points are in eclipse using the formulation given in Ref. [23]. Given the position of the spacecraft and the Sun relative to the Earth, Ref. [23] calculates an eclipse value that is 0 in eclipse, 1 in sunlight, and (0, 1) in the penumbra.

### *3.1.2 RAAN matching method*

This method builds on the extended Edelbaum method such that RAAN changing transfers can be optimized. In this method, orbital precession is used to achieve a target RAAN by phasing at an intermediate phasing orbit, as

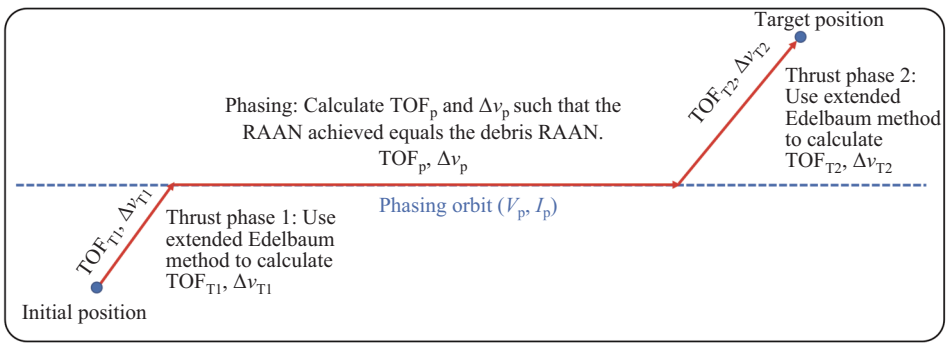


**Fig. 2** Thrust–phasing–thrust structure (subscript T1 denotes the first thrust phase, subscript p denotes phasing, and subscript T2 indicates the second thrust phase).

**Algorithm 1** Extended Edelbaum method

**Require:** Initial and final orbital velocity $(V_0, V_\mathrm{f})$, change in inclination $\Delta i$, maximum thrust $(T_\mathrm{max})$

Calculate $\Delta v$ and mission TOF $(t_\mathrm{f})$ using Eqs. (1) and (2):

$$\Delta v_\mathrm{total} = \sqrt{V_0^2 + V_\mathrm{f}^2 - 2V_0 V_\mathrm{f}\cos(\pi/2\Delta i)} \tag{1}$$

$$t_\mathrm{f} = \frac{\Delta v_\mathrm{total}}{T} \tag{2}$$

Calculate the initial yaw steering angle $\beta_0$, defined in the plane normal to the orbit plane, using Eq. (3):

$$\tan\beta_0 = \frac{\sin(\pi/2\Delta i)}{\frac{V_0}{V_\mathrm{f}} - \cos(\pi/2\Delta i)} \tag{3}$$

Calculate thrust acceleration $f_\mathrm{t} = \frac{T_\mathrm{max}}{m_0}$.

Discretize the TOF $(t_\mathrm{f})$ into $N$ segments and compute the semi-major axis, inclination, yaw steering angle $\beta(t)$, and $\Delta v$ per segment using Eqs. (4), (5), (6), and (2), respectively.

$$a(t) = \frac{\mu}{V_0^2 + f_\mathrm{t}^2 t^2 - 2V_0 f_\mathrm{t} t\cos(\beta_0)} \tag{4}$$

$$i(t) = i_0 + \mathrm{sgn}(i_\mathrm{f} - i_0)\frac{2}{\pi}\left(\arctan\left(\frac{f_\mathrm{t}t - V_0\cos\beta_0}{V_0\sin\beta_0}\right) + \frac{\pi}{2} - \beta_0\right) \tag{5}$$

$$\beta(t) = \arctan\left(\frac{V_0\sin\beta_0}{V_0\cos\beta_0 - f_\mathrm{t}t}\right) \tag{6}$$

**for** $k = 1 : N$ **do**

Calculate the sunlit time during a single orbit $(w_\mathrm{ecl})$ using the eclipse time formulation in Ref. [23].

Calculate the fraction of thrust time per orbit $(w)$.

$$w(k) = \min[\mathrm{DC}, w_\mathrm{ecl}],\ \text{where DC : duty cycle} \tag{7}$$

Calculate mass $m(k)$ using $\Delta v(k)$ and the rocket equation.

Calculate $f_\mathrm{t}(k) = T_\mathrm{max}/m(k)$

Compute the new transfer time using Eq. (8):

$$t(k+1) = t(k) + \frac{\Delta v(k+1) - \Delta v(k)}{f_\mathrm{t}(k)w(k)} \tag{8}$$

Calculate drag acceleration $(f_\mathrm{d})$ at $t_k$ using Eq. (9):

$$f_\mathrm{d} = -\frac{1}{2}\frac{\rho C_\mathrm{d} A v(k)^2}{m(k)} \tag{9}$$

where $\rho, C_\mathrm{d}, A, v(k)$, and $m(k)$ represent the air density, drag coefficient, frontal area, velocity, and mass, respectively.

Calculate the semi major axes $a_\mathrm{d}(k+1)$ from $f_\mathrm{d}(k)$ using Eq. (4), assuming $f_\mathrm{d}(k)$ remains constant from $t_k$ to $t_{k+1}$.

Update $a(k+1) \leftarrow a(k+1) - (a(k) - a_\mathrm{d}(k+1))$.

Return to the first step of this algorithm and repeat the procedure from $t(k+1)$ to $t_\mathrm{f}$.

Propagate the RAAN using Eqs. (10) and (11):

$$\dot{\Omega}(k) = -\frac{3}{2}J_2\sqrt{\frac{\mu}{a(k)^3}}\left(\frac{R_\mathrm{e}}{a(k)}\right)^2\cos i \tag{10}$$

$$\Omega(k+1) = \Omega(k) + \dot{\Omega}(k)(t(k+1) - t(k)) \tag{11}$$

**end for**

conducted in Ref. [11]. Note that in the thrust phases, Edelbaum's model is used to determine the optimal thrust, which maintains the thrust direction at a constant angle with respect to the orbital plane, switching signs at the antinodes. Thus, the thrust has no direct impact on the RAAN [24]. The spacecraft follows the thrust–

phasing–thrust trajectory shown in Fig. 2 to reach its target state. The phasing orbit variables ($V_\mathrm{p}$ and $I_\mathrm{p}$) are obtained by optimizing the transfer for optimal time or propellant consumption, as discussed in Section 3.1.3.

During phasing, some thrust may be required to maintain the orbital altitude. Hence, the thrust magnitude is set to be equal to the drag acceleration experienced. The thrust direction is set act in the opposite direction of the drag. The two thrust phases in this sequence are evaluated using the extended Edelbaum method discussed earlier. Algorithm 2 shows the steps associated with calculating the TOF and $\Delta v$ for a trajectory that utilizes the RAAN matching method. Note that $\Omega_{t_0,\mathrm{initial}}$ and $\Omega_{t_0,\mathrm{target}}$ are the RAANs of the spacecraft and target at the start of the transfer, respectively.

### *3.1.3 Optimization*

Consider a mission that aims to remove a set of debris from debris(1) to debris($N$). The optimization of this mission is initiated from the orbit of debris(1), as the initial orbit of the Servicer prior to that point is not well-defined. First, the Servicer brings debris(1) down to the Shepherd. The TOF and $\Delta v$ consumed in this phase are calculated using the extended Edelbaum method. Next, the debris is handed over to the Shepherd. The handover is expected to take $\mathrm{TOF}_\mathrm{handover}$. During this time, the influence of $J_2$ on RAAN is considered in the optimization. Subsequently, the Servicer returns to collect debris(2), for which time and fuel consumption are calculated using the RAAN matching method. Proximity operations are performed in the vicinity of debris(2), such

**Algorithm 2** RAAN matching method

**Require:** Initial orbit elements ($a_0$, $i_0$, $\Omega_{t_0,\mathrm{initial}}$), target orbit elements ($a_\mathrm{f}$, $i_\mathrm{f}$, $\Omega_{t_0,\mathrm{target}}$), and phasing orbit elements ($V_\mathrm{p}, I_\mathrm{p}$).

**Thrust phase 1**

Input: $a_0$, $i_0$, $V_\mathrm{p}$, and $I_\mathrm{p}$

Calculate $\mathrm{TOF}_{\mathrm{T}1}$ and $\Delta v_{\mathrm{T}1}$ using the extended Edelbaum method. Calculate $\Delta\Omega_{\mathrm{T}1}$ (RAAN change of the spacecraft due to precession during thrust phase 1).

Output: $\mathrm{TOF}_{\mathrm{T}1}$, $\Delta v_{\mathrm{T}1}$, and $\Delta\Omega_{\mathrm{T}1}$.

**Thrust phase 2**

Input: $V_\mathrm{p}$, $I_\mathrm{p}$, $a_\mathrm{f}$, and $i_\mathrm{f}$

Calculate $\mathrm{TOF}_{\mathrm{T}2}$ and $\Delta v_{\mathrm{T}2}$ using the extended Edelbaum method. Calculate $\Delta\Omega_{\mathrm{T}2}$ (RAAN change of the spacecraft due to precession during thrust phase 2).

Output: $\mathrm{TOF}_{\mathrm{T}2}$, $\Delta v_{\mathrm{T}2}$, and $\Delta\Omega_{\mathrm{T}2}$.

**Phasing**

Input: $V_\mathrm{p}$, $I_\mathrm{p}$, $a_\mathrm{f}$, $i_\mathrm{f}$, $\mathrm{TOF}_{\mathrm{T}1}$, $\mathrm{TOF}_{\mathrm{T}2}$, $\Delta\Omega_{\mathrm{T}1}$, $\Delta\Omega_{\mathrm{T}2}$, $\Omega_{t_0,\mathrm{initial}}$, and $\Omega_{t_0,\mathrm{target}}$

Calculate the phasing rate of the spacecraft $\dot{\Omega}_{\mathrm{s/c}}$ and the phasing rate of the target $\dot{\Omega}_\mathrm{target}$ using Eq. (10).

Calculate $\mathrm{TOF}_\mathrm{p}$ (phasing time required to match with the final RAAN) using Eq. (12), which equates the RAAN reached by the Servicer to the RAAN of the debris at arrival time.

$$\Omega_{t_0,\mathrm{initial}} + \Delta\Omega_{\mathrm{T}1} + \Delta\Omega_{\mathrm{T}2} + \dot{\Omega}_{\mathrm{s/c}}\mathrm{TOF}_\mathrm{p} = \Omega_{t_0,\mathrm{target}} + \dot{\Omega}_\mathrm{target}\left(\mathrm{TOF}_\mathrm{p} + \mathrm{TOF}_{\mathrm{T}1} + \mathrm{TOF}_{\mathrm{T}2}\right) \tag{12}$$

Calculate the $\Delta v$ used to offset the drag in the phasing phase ($\Delta v_\mathrm{p}$). This is achieved by setting the thrust magnitude equal to the drag acceleration (Eq. (9)) acting in the opposite direction during phasing. Subsequently,

$$\Delta v_\mathrm{p} = -\int_0^{\mathrm{TOF}_\mathrm{p}} f_\mathrm{d}\mathrm{d}t \tag{13}$$

Output: $\mathrm{TOF}_\mathrm{p}$ and $\Delta v_\mathrm{p}$

**Return**: Calculate the total $\Delta v$ and TOF.

$$\Delta v = \Delta v_{\mathrm{T}1} + \Delta v_{\mathrm{T}2} + \Delta v_\mathrm{p} \tag{14}$$

$$\mathrm{TOF} = \mathrm{TOF}_{\mathrm{T}1} + \mathrm{TOF}_\mathrm{p} + \mathrm{TOF}_{\mathrm{T}2} \tag{15}$$

that it can rendezvous with the Servicer. This process is assumed to take $\mathrm{TOF}_{\text{prox-ops}}$. Then, debris(2) is carried to the Shepherd, and the time and fuel consumption for this is calculated using the extended Edelbaum method. This process is repeated for all debris in the sequence. Figure 3 illustrates this in detail.

The phasing orbit parameters and the launch epoch of the mission must be optimized to obtain the best TOF or $\Delta v$ for a given tour. The input parameters required for the optimization are the duty cycle, maximum thrust, specific impulse, constraints on TOF or $\Delta v$, coordinates of the debris to be removed, Servicer wet mass, and optimization parameter (TOF or $\Delta v$).

The optimization vector ($\boldsymbol{x}$) is set to represent the orbital velocity $V$ and the inclination $I$ of all phasing orbits in the tour. Thus, for a sequence of $N$ debris,

$$\boldsymbol{x} = \left[V_{\mathrm{p}_1}, I_{\mathrm{p}_1}, V_{\mathrm{p}_2}, I_{\mathrm{p}_2}, \ldots, V_{\mathrm{p}_{N-1}}, I_{\mathrm{p}_{N-1}}\right] \tag{16}$$

Note that the second subscript plus one is the debris that is reached using that phasing orbit (i.e., $[V_{\mathrm{p}_1}, I_{\mathrm{p}_1}]$ is used to reach debris(2), etc.). Figure 3 shows the steps involved in the objective function calculation to remove $N$ debris. The optimization uses the interior-point algorithm in MATLAB's *fmincon*. As either TOF or $\Delta v$ is being optimized in a given simulation, constraints can be set on the other parameter such that it remains within a feasible domain. These constraints are introduced as nonlinear inequality constraints to the optimization.

### 3.2 Mission guidance

The PMDT can provide only a low-accuracy solution to the optimal trajectories as no integration of the dynamics is conducted. If the thrust law computed with the PMDT is applied in a forward manner, the trajectory can deviate significantly from the reference owing to the simplifications made in the model and the lack of a feedback mechanism. These limitations can be circumvented by the inclusion of a guidance scheme that computes the thrust law to track the PMDT reference trajectory. The guidance scheme can aid in assessing the accuracy of the PMDT and provides a method to actually fly the mission.

Three such schemes are explored for this: the first one adapts the guidance laws by Ruggiero in Ref. [14], the second utilizes the $\Delta v$-law proposed by Locoche in Ref. [15], and the third one uses the Q-law proposed by Petropolous in Ref. [16]. Note that these laws take the transfers computed by the PMDT as references to track, which enables them to also use $J_2$ to minimize fuel consumption due to RAAN changes. This feature is not directly available in these schemes.

Importantly, these laws take the transfers computed from PMDT as references to track, thus implicitly exploiting $J_2$, a feature not directly available in these schemes.

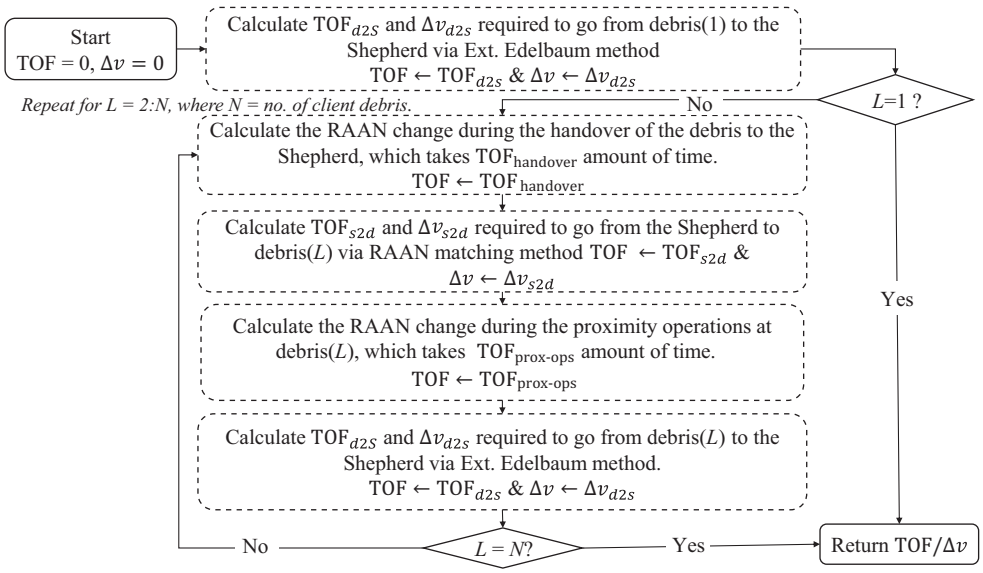


**Fig. 3** Fitness function calculation for the optimization.

### *3.2.1 Ruggiero guidance*

The Ruggiero guidance was proposed by Ruggiero in Ref. [14]. It uses a closed loop guidance law to steer a given orbital element to a target value. Hence, the thrust direction is changed according to the orbital element correction laws generated based on the optimal thrust direction $\boldsymbol{f}_{\mathrm{t}}$ given in Table 1 in Ref. [14]. Denoting the current orbital elements as $\boldsymbol{X} = [a, e, i, \Omega]^{\mathrm{T}}$ and the target elements as $\boldsymbol{X}_{\mathrm{T}} = [a_{\mathrm{T}}, e_{\mathrm{T}}, i_{\mathrm{T}}, \Omega_{\mathrm{T}}]^{\mathrm{T}}$, the optimal thrust vectors for changing each orbital element are

- Semi-major axis ($a$):

$$\boldsymbol{f}_{\mathrm{t}_a} = (\eta_a > \eta_a^{bd})\,\mathrm{sgn}(a_{\mathrm{T}} - a) \cdot [\cos\beta_a \sin\alpha_a, \cos\beta_a \cos\alpha_a, \sin\beta_a] \quad (17)$$

where

$$\tan\alpha_a = \frac{e\sin\nu}{1 + e\cos\nu}, \beta_a = 0, \eta_a = |\boldsymbol{v}|\sqrt{\frac{a(1-e)}{\mu(1+e)}}$$

- Eccentricity ($e$):

$$\boldsymbol{f}_{\mathrm{t}_e} = (\eta_e > \eta_e^{bd})\,\mathrm{sign}(e_{\mathrm{T}} - e) \cdot [\cos\beta_e \sin\alpha_e, \cos\beta_e \cos\alpha_e, \sin\beta_e] \quad (18)$$

where

$$\tan\alpha_e = \frac{\sin\nu}{\cos E + \cos\nu}, \beta_e = 0,$$
$$\eta_e = \frac{1 + 2e\cos\nu + \cos^2\nu}{1 + e\cos\nu}$$

- Inclination ($i$):

$$\boldsymbol{f}_{\mathrm{t}_i} = (\eta_i > \eta_i^{bd})\,\mathrm{sgn}(i_{\mathrm{T}} - i) \cdot [\cos\beta_i \sin\alpha_i, \cos\beta_i \cos\alpha_i, \sin\beta_i] \quad (19)$$

where

$$\tan\alpha_i = 0, \beta_i = \frac{\pi}{2}\,\mathrm{sgn}(\cos(\omega + \nu)),$$
$$\eta_i = \frac{|\cos(v+\omega)|}{1 + e\cos v}\left(\sqrt{1 - e^2\sin^2\omega} - e|\omega|\right)$$

- Right ascension of the ascending node ($\Omega$):

$$\boldsymbol{f}_{\mathrm{t}_\Omega} = (\eta_\Omega > \eta_\Omega^{bd})\,\mathrm{sgn}\left(\frac{-\sin(\Omega - \Omega_{\mathrm{T}})}{\sqrt{1 - \cos^2(\Omega - \Omega_{\mathrm{T}})}}\right) \cdot [\cos\beta_\Omega \sin\alpha_\Omega, \cos\beta_\Omega \cos\alpha_\Omega, \sin\beta_\Omega] \quad (20)$$

where

$$\tan\alpha_\Omega = 0, \beta_\Omega = \frac{\pi}{2}\,\mathrm{sgn}(\sin(\omega + \nu)),$$
$$\eta_\Omega = \frac{|\sin(\nu+\omega)|}{1 + e\cos\nu}\left(\sqrt{1 - e^2\cos^2\nu} - e|\sin\omega|\right)$$

(Note that the term $\mathrm{sgn}\left(\frac{-\sin(\Omega-\Omega_{\mathrm{T}})}{\sqrt{1-\cos^2(\Omega-\Omega_{\mathrm{T}})}}\right)$ is used instead of $\mathrm{sgn}(\Omega_{\mathrm{T}} - \Omega)$ to determine the direction of the thrust required to go towards $\Omega_{\mathrm{T}}$. This is performed to obtain the correct direction with the smallest angle between $\Omega$ and $\Omega_{\mathrm{T}}$.)

The thrust vector is only activated above the limits set by $\eta^{bd}$. At each time step of the tour, the orbital elements from the PMDT solution are taken as the target when providing guidance.

When the optimal thrust vectors are calculated, weighting coefficients ($c_X$) are introduced to alter the intrinsic behavior and prioritize certain orbital elements. Then, the optimal unit thrust acceleration ($\boldsymbol{u}$) can be calculated as Eq. (21):

$$\hat{\boldsymbol{f}}_{\mathrm{t,opt}} = \frac{c_a\boldsymbol{f}_{\mathrm{t}_a} + c_e\boldsymbol{f}_{\mathrm{t}_e} + c_i\boldsymbol{f}_{\mathrm{t}_i} + c_\Omega\boldsymbol{f}_{\mathrm{t}_\Omega}}{|c_a\boldsymbol{f}_{\mathrm{t}_a} + c_e\boldsymbol{f}_{\mathrm{t}_e} + c_i\boldsymbol{f}_{\mathrm{t}_i} + c_\Omega\boldsymbol{f}_{\mathrm{t}_\Omega}|} \quad (21)$$

where $c_X = |X - X_{\mathrm{T}}|W_x$.

For each element in $\boldsymbol{X}$, $c_X$ is dependent on the difference between the current value of the orbital element and the target value. $\boldsymbol{W} = [W_a, W_e, W_i, W_\Omega]^{\mathrm{T}}$ are coefficients to be optimized to improve the performance of Ruggiero guidance.

### *3.2.2 $\Delta v$-law*

The $\Delta v$-law guidance scheme called the $\Delta v$-law, proposed by Lococche in Ref. [15], is based on Lyapunov feedback control. This method entails developing a control feedback algorithm that decreases a scalar function (called the Lyapunov function), representing the distance between the current state and its target. The designed control algorithm aims to drive the Lyapunov function ($L$) to zero. The $L$ function used in the $\Delta v$-law is

$$L = \widetilde{\Delta v}^2 \equiv \lambda_a\left(V_{\mathrm{c}}^2 - 2V_{\mathrm{c}}V_{\mathrm{cf}}\cos(\pi/2\Delta\sigma) + V_{\mathrm{cf}}^2\right) + \frac{4}{9}\lambda_{e_1}\left\{\frac{[(1-\lambda_{e_2})V_{\mathrm{c}} + \lambda_{e_2}V_{\mathrm{cf}}]\,(\arcsin(e) - \arcsin(e_{\mathrm{f}}))}{\cos(\widetilde{\beta})}\right\}^2 \quad (22)$$

where

$$\Delta\sigma = \sqrt{(\lambda_{a,i}\Delta i)^2 + (\lambda_{a,\Omega}\sin(i)\Delta\Omega)^2}$$
$$\tan(|\tilde{\beta}|) = \left|\frac{3\pi\lambda_{e,i}\Delta i}{4\cos(\lambda_\omega\omega)\left(\ln\left(\frac{e_{\mathrm{f}}+1}{e_{\mathrm{f}}-1}\right) + \ln\left(\frac{e-1}{e+1}\right) - \Delta e\right)}\right| \quad (23)$$

Here, $V_{\mathrm{c}}$ and $V_{\mathrm{f}}$ indicate the current and target orbital velocities respectively. $\lambda_{e_1}, \lambda_{e_2}, \lambda_{a,i}, \lambda_{e,i}, \lambda_{a,\Omega}$, and $\lambda_\omega$ are parameters to be optimized to enhance the Lyapunov controller performance. Note that $L$ is constructed by combining the analytical $\Delta v$ equations to perform semi-major axis, eccentricity, inclination, and RAAN changes [15]. Additionally, note that $\Delta i = i - i_{\mathrm{T}}$, $\Delta\Omega = \arccos(\cos(\Omega - \Omega_{\mathrm{T}}))$, and $\Delta e = e - e_{\mathrm{T}}$.

The aim of Lyapunov control is to make $\dot{L}$ as negative as possible such that $L$ will approach zero quickly. Note that

$$\dot{L} = \frac{\partial L}{\partial \boldsymbol{X}}\dot{\boldsymbol{X}} = \frac{\partial L}{\partial \boldsymbol{X}}\boldsymbol{B}\boldsymbol{f}_{\mathrm{t}} \tag{24}$$

where $\boldsymbol{X}$ denotes the state variables as given in Ruggiero guidance, and $\boldsymbol{B}$ represents the Gauss variational equations (GVEs) for the slow variables and is given by

$$\boldsymbol{B} = \begin{bmatrix} \frac{2a^2}{h}e\sin(\nu) & \frac{2a^2}{h}\frac{p}{r} & 0 \\ \frac{1}{h}p\sin(\nu) & \frac{1}{h}[(p+r)\cos(\nu)+re] & 0 \\ 0 & 0 & \frac{r\cos(\omega+\nu)}{h} \\ 0 & 0 & \frac{r\sin(\omega+\nu)}{h\sin(i)} \end{bmatrix} \tag{25}$$

Hence, the optimal control acceleration direction can be calculated as

$$\hat{\boldsymbol{f}}_{\mathrm{t,opt}} = -\frac{\boldsymbol{B}^{\mathrm{T}}\left(\frac{\partial L}{\partial \boldsymbol{X}}\right)^{\mathrm{T}}}{\left\|\left(\frac{\partial L}{\partial \boldsymbol{X}}\right)\boldsymbol{B}\right\|} \tag{26}$$

### *3.2.3 Q-law*

One of the most versatile and well-known control laws is the Q-law developed by Petropoulos [16]. The Q-law is best thought of as a weighted, squared summation of the time required to change the current state $\boldsymbol{X} = [a, e, i, \Omega]^{\mathrm{T}}$ to the target state $\boldsymbol{X}_{\mathrm{T}} = [a_{\mathrm{T}}, e_{\mathrm{T}}, i_{\mathrm{T}}, \Omega_{\mathrm{T}}]^{\mathrm{T}}$. It can be expressed as

$$Q = (1 + W_P P(\boldsymbol{X}))\sum_X S_X(\boldsymbol{X})W_X(\boldsymbol{X})\left(\frac{\delta(X, X_{\mathrm{T}})}{\max_\nu(\dot{X})}\right)^2 \tag{27}$$

where $W_P$ and $P$ form a penalty function, and $S_X$ are scaling functions. These are functions of the state and are described in Ref. [16]. $\delta(X, X_{\mathrm{T}}) = X - X_{\mathrm{T}}$ for $X = a, e, i$, whereas $\delta(X, X_{\mathrm{T}}) = \arccos(\cos(X - X_{\mathrm{T}}))$ for $X = \Omega$. The expressions $\max_\nu(\dot{X})$ denote the maximum rate of change of each COE over the current osculating orbit and can be calculated analytically for all elements. The weights $W_X$ can be used to prioritize which elements to target.

$$\dot{Q} = \frac{\partial Q}{\partial \boldsymbol{X}}\dot{\boldsymbol{X}} = \frac{\partial Q}{\partial \boldsymbol{X}}\boldsymbol{B}\boldsymbol{f}_{\mathrm{t}} \tag{28}$$

leading to a control acceleration direction

$$\hat{\boldsymbol{f}}_{\mathrm{t,opt}} = -\frac{\boldsymbol{B}^{\mathrm{T}}\left(\frac{\partial Q}{\partial \boldsymbol{X}}\right)^{\mathrm{T}}}{\left\|\left(\frac{\partial Q}{\partial \boldsymbol{X}}\right)\boldsymbol{B}\right\|} \tag{29}$$

### *3.2.4 Propagating with guidance*

**(1) Integrating the effect of eclipses and duty cycle.**

When propagating the dynamics with guidance, the effect of eclipses and duty cycle must be considered adequately. However, turning thrust off asymmetrically (i.e., only during the eclipse) will cause eccentricity to build up [13]. Hence, thrust is turned off symmetrically across the orbit in the highlighted regions in Fig. 4. These regions are determined as follows.

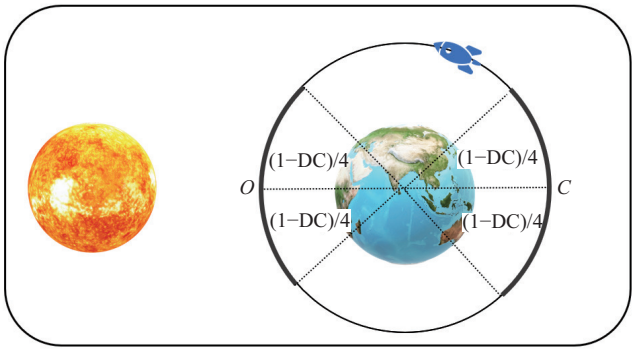


**Fig. 4** Eclipse formulation for propagating with guidance.

First, the value of the argument of latitude at the eclipse center ($\theta_C$) is calculated at each time step of the propagation. Next, the thrust is turned off for a symmetric fraction of the orbit across the point $C$ when $\theta_C - 2\pi\frac{1-\mathrm{DC}}{4} \leqslant \theta \leqslant \theta_C + 2\pi\frac{1-\mathrm{DC}}{4}$, where DC is the duty cycle. The thrust is also turned off for the same orbit fraction opposite from $C$ (at $O$), when $\theta_O - 2\pi\frac{1-\mathrm{DC}}{4} \leqslant \theta \leqslant \theta_O + 2\pi\frac{1-\mathrm{DC}}{4}$.

Note that if the spacecraft were required to make large inclination changes and one of the orbit nodes lay within the eclipse, thrusting can be performed on the opposite side of the eclipse to make inclination changes more efficient. Depending on the power budget, thrust can also be provided during the eclipse. The build-up of eccentricity incurred by asymmetric thrusting can be corrected by guidance.

**(2) Counteracting drag in phasing orbits.**

Note that using guidance during the phasing orbits for RAAN matching uses a large amount of propellant to counteract minute orbital changes resulting from the drag. To minimize this, the thrust is only turned on when the drag results in significant orbit changes compared with the reference phasing orbit. Hence, on phasing orbits, the thrust is only turned on when $|a - a_{\mathrm{ref}}| > 5$ km, $|i - i_{\mathrm{ref}}| > 0.1$ deg, or $|\Omega - \Omega_{\mathrm{ref}}| > 0.1$ deg provided that the spacecraft is not in eclipse. The thrust is turned off when $|a - a_{\mathrm{ref}}| < 0.5$ km, $|i - i_{\mathrm{ref}}| < 0.01$ deg, and $|\Omega - \Omega_{\mathrm{ref}}| < 0.01$ deg to conserve fuel.

Algorithm 3 illustrates the implementation of the three guidance schemes when propagating the dynamics. Note that the mean orbital elements are used to calculate the control acceleration direction such that propellant is not wasted on correcting for the osculating nature of the elements.

The GVEs are used to propagate the dynamics.

$$\begin{aligned}
\frac{\mathrm{d}a}{\mathrm{d}t} &= 2\frac{a^2}{\sqrt{\mu p}}\left(f_{\mathrm{R}} e\sin\nu + f_{\mathrm{T}}\frac{p}{r}\right)\\
\frac{\mathrm{d}e}{\mathrm{d}t} &= \sqrt{\frac{p}{\mu}}\left[f_{\mathrm{R}}\sin\nu + f_{\mathrm{T}}(\cos E + \cos\nu)\right]\\
\frac{\mathrm{d}i}{\mathrm{d}t} &= f_{\mathrm{N}}\frac{r}{\sqrt{\mu p}}\cos(\nu+\omega)\\
\frac{\mathrm{d}\omega}{\mathrm{d}t} &= -\sqrt{\frac{p}{\mu}}\left\{f_{\mathrm{N}}\frac{r}{p}\cot i\sin(\nu+\omega)\right.\\
&\quad \left.+\frac{1}{e}\left[f_{\mathrm{R}}\cos\nu - f_{\mathrm{T}}\left(1+\frac{r}{p}\right)\sin\nu\right]\right\}\\
\frac{\mathrm{d}\Omega}{\mathrm{d}t} &= f_{\mathrm{N}}\frac{r}{\sqrt{\mu p}\sin i}\sin(\nu+\omega)
\end{aligned}$$

$$\begin{aligned}
\frac{\mathrm{d}M}{\mathrm{d}t} &= n - f_{\mathrm{R}}\left(\frac{2r}{\sqrt{\mu a}} - \frac{1-e^2}{e}\sqrt{\frac{a}{\mu}}\cos\nu\right)\\
&\quad - f_{\mathrm{T}}\frac{1-e^2}{e}\sqrt{\frac{a}{\mu}}\left(1+\frac{r}{p}\right)\sin\nu
\end{aligned} \tag{32}$$

where $p$ is the semi latus rectum $p = a(1-e^2)$, and $f_{\mathrm{R}}, f_{\mathrm{T}}$, and $f_{\mathrm{N}}$ are the perturbing accelerations in the RTN frame. Note that

$$\boldsymbol{f} = \begin{bmatrix} f_{\mathrm{R}} \\ f_{\mathrm{T}} \\ f_{\mathrm{N}} \end{bmatrix} = \boldsymbol{f}_{J2} + \boldsymbol{f}_{\mathrm{d}} + \boldsymbol{f}_{\mathrm{t}} \tag{33}$$

where $J_2$ acceleration $\boldsymbol{f}_{J2}$, and drag acceleration $\boldsymbol{f}_{\mathrm{d}}$ are calculated as described in Ref. [25]. $\boldsymbol{f}_{\mathrm{t}} = \eta\frac{T_{\max}}{m}\hat{\boldsymbol{f}}_{\mathrm{t,opt}}$, where $\eta$ is the eclipse factor and $\hat{\boldsymbol{f}}_{\mathrm{t,opt}}$ is the optimal thrust acceleration direction provided by the guidance or the PMDT (where $\hat{\boldsymbol{f}}_{\mathrm{t,opt}} = [0, \cos\beta, \sin\beta]$).

### *3.2.5 Optimizing the guidance parameters*

Each of the three guidance approaches has user-defined parameters in the form of weights: $W_x$ for Ruggiero and the Q-law guidance, and $\lambda_x$ for the $\Delta v$-law guidance.

**Algorithm 3** Implementation of guidance

**Require:** The PMDT solution of the transfer, the transfer time ($t_{\mathrm{f}}$).

**for** $t = 0 : t_{\mathrm{f}}$ **do**

1. Convert the osculating orbital elements to mean elements.
2. Calculate the target state ($\boldsymbol{X}_{\mathrm{T}}$) at $t$ by interpolating the PMDT solution.
3. Calculate the optimal thrust direction ($\boldsymbol{u}$) using Eq. (21) (For Ruggiero guidance), Eq. (26) (for $\Delta v$-law guidance) or Eq. (29) (for Q-law guidance), taking the mean elements as the current state.
4. Calculate the effect of the eclipse and duty cycle.

**if** $(\theta_C - 2\pi\frac{1-\mathrm{DC}}{4} \leqslant \theta \leqslant \theta_C + 2\pi\frac{1-\mathrm{DC}}{4}$ **or** $\theta_O - 2\pi\frac{1-\mathrm{DC}}{4} \leqslant \theta \leqslant \theta_O + 2\pi\frac{1-\mathrm{DC}}{4})$ **then**
$\eta = 0$
**else**
$\eta = 1$
**end if**

5. If propagating a phasing orbit, implement the drag counteraction method.

**if** ( $|a - a_{\mathrm{ref}}| > 5$ km **or** $|i - i_{\mathrm{ref}}| > 0.1$ deg **or** $|\Omega - \Omega_{\mathrm{ref}}| > 0.1$ **and** $\eta \neq 0$) **then**
$\eta = 1$
**else if** ($|a - a_{\mathrm{ref}}| < 0.5$ km **and** $|i - i_{\mathrm{ref}}| < 0.01$ deg **and** $|\Omega - \Omega_{\mathrm{ref}}| < 0.01$ deg) **then**
$\eta = 0$
**end if**

6. Use Eq. (32) to determine the time derivative of the state $\dot{\boldsymbol{X}}$, where

$$\dot{\boldsymbol{X}} = [\dot{a}, \dot{e}, \dot{i}, \dot{\omega}, \dot{\Omega}, \dot{M}]^{\mathrm{T}} \tag{30}$$

7. Determine the derivative of the mass by

$$\dot{m} = \frac{T_{\max}}{I_{sp} g_0} \tag{31}$$

**end for**

Integrate $\dot{\boldsymbol{X}}$ to obtain $\boldsymbol{X}$ using a propagator such as MATLAB's *ode45*.

These parameters can significantly affect the behavior of the guidance control laws. Thus, particle swarm optimization (PSO) is used to tune these parameters. Due to the computational challenges of converting from osculating to mean elements and computing the duty cycle, the guidance strategy was simplified for the PSO.

A duty cycle of 50% was simulated by reducing the spacecraft thrust by a factor of 2. In addition, only the average/secular contribution of $J_2$ was considered, removing the requirement for converting from osculating to mean elements when computing the control. Given that there are two distinct transfer scenarios, either lowering the altitude with the debris attached to the Servicer or climbing and rendezvousing to the debris, different sets of weights were computed for these two transfer scenarios. This further reduced the computational requirements and created a design vector of maximum 10 elements, five for the downward legs and five for the upwards legs. For the Ruggiero and Q-law guidance, the weights relating to the eccentricity and argument of periapsis can automatically be set to 0. For Lococh guidance, the problem can be simplified by assuming $\lambda_\omega = 0$ as the eccentricity and the argument of periapsis are not targeted.

Six PSO simulations were initiated, with a swarm size of 50 each, tracking the time- and fuel-optimal reference trajectories with the Ruggiero, $\Delta v$-law, and Q-law guidance strategies. Whilst tracking the reference trajectory, the objective was to minimize the accumulated errors in the semi-major axis, inclination, and RAAN at the end of each leg. When a set of weights were obtained in the simplified scenarios used in the PSO, there were deployed in the original, osculating dynamics with the 50% duty cycle. The coefficients provided by these PSO simulations are reported in Tables 3 and 7 in Sections 4.1 and 4.2, respectively. Naturally, a deviation from the PSO results was observed, but the guidance remained satisfactory without requiring extensive computational resources. Note that the results might be improved upon with a more accurate model in the PSO simulations, at the cost of increasing the computational effort.

## 4 Exemplar three-debris ADR mission

This section discusses the results of optimizing an ADR mission for three debris in near Sun-synchronous orbits. The objects to be removed were, in order, H-2A R/B (ID: 33500), ALOS 2 (ID: 39766), and GOSAT (ID: 33492). The masses of these objects were taken to be 2991, 2120, and 1750 kg, respectively.

This sequence of objects was selected arbitrarily to provide an exemplar test case in which PMDT could be evaluated. Note that the debris sequence can be optimized using the PMDT to asses various sequences, but this was not performed in this preliminary study.

The propulsion conditions used were 60 mN maximum thrust, 50% duty cycle, and 1300 s specific impulse. The Servicer was assumed to have a wet mass of 800 kg, and the launch date was set to 25-Mar-2022 06:37:09 UTC. The debris two-line elements (TLEs) were obtained from 31-Aug-2021 to 15-Dec-2021. Ephemeris kernels were generated using MKPSK[③], extrapolating the states outside the TLE time window, to make data available for the phases of the mission following the launch in 2022. Thus, the total epoch considered was from the first TLE date until three years after the final TLE. The altitude at which the debris and the Servicer meet the Shepherd was set to 350 km, i.e., below the ISS altitude, to satisfy safety requirements. Eclipses and drag acceleration were considered for this case study. $\mathrm{TOF}_{\mathrm{prox\text{-}op}}$ and $\mathrm{TOF}_{\mathrm{handover}}$ were set to be 45 and 30 days, respectively.

The optimizations were conducted on MATLAB 2022b using a Windows Desktop computer with an Intel Core i7-117000 CPU of 2.50 GHz and 32.0 GB of RAM.

### 4.1 Fuel-optimal scenario

When generating the fuel-optimal result, the total TOF was limited to less than five years (1825 days). The initial phasing orbit guess required to solve the fuel-optimal trajectory using fmincon was set to be the average between the final and initial velocity and inclination of each of the transfers that require phasing. In the optimized solution, the first phasing orbit (going from the Shepherd altitude to ALOS 2) was at $a = 7662.8$ km and $i = 98.29$ deg. The second optimal phasing orbit (going from the Shepherd altitude to GOSAT) was at $a = 7499.2$ km and $i = 97.85$ deg. The optimization took 10.41 s to complete. The optimal $\Delta v$ obtained was 945.58 m/s, with a total fuel consumption of 136.07 kg. Note that the optimized tour requires five years, i.e., it is at the limit for the total allowed TOF. Tours with better

③ https://naif.jpl.nasa.gov/pub/naif/toolkit_docs/C/ug/mkspk.html

**Table 1** Orbital elements of the target debris at launch time

| Debris | $a$ (km) | $e$ | $i$ (deg) | $\Omega$ (deg) | $\omega$ (deg) | $M$ (deg) |
|---|---|---|---|---|---|---|
| H-2A R/B | 6986.160 | 0.00468 | 98.146 | 20.248 | 180.154 | 335.561 |
| ALOS 2 | 7008.582 | 0.00144 | 97.918 | 182.340 | 116.123 | 281.396 |
| GOSAT | 7052.974 | 0.00101 | 98.062 | 197.538 | 73.893 | 279.245 |

**Table 2** Fuel-optimal tour: $\Delta v$ and TOF per leg

| Leg | $\Delta v$ (m/s) | TOF (d) |
|---|---|---|
| Leg 1 (from H-2A R/B to 350 km orbit) | 140.12 | 203.82 |
| Handover | — | 30.00 |
| Leg 2 (from 350 km orbit to ALOS 2) | 238.54 | 817.44 |
| Proximity operations | — | 45.00 |
| Leg 3 (from ALOS 2 to 350 km orbit) | 151.93 | 166.91 |
| Handover | — | 30.00 |
| Leg 4 (from 350 km orbit to GOSAT) | 239.86 | 292.57 |
| Proximity operations | — | 45.00 |
| Leg 5 (from GOSAT to 350 km orbit) | 175.14 | 164.25 |
| Handover | — | 30.00 |
| Total | 945.58 | 1825.00 |

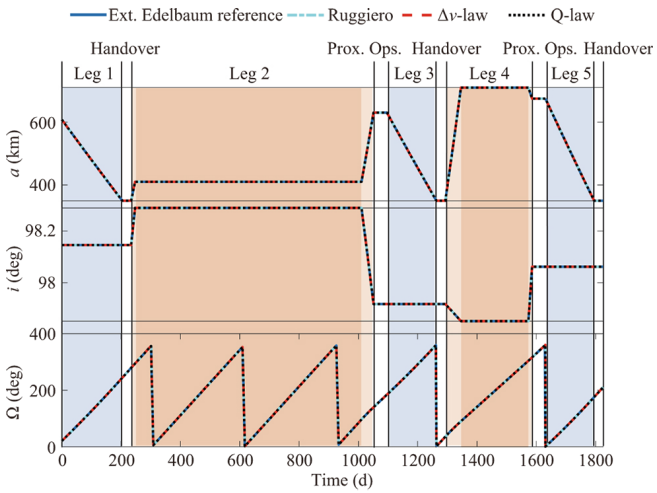


**Fig. 5** Fuel-optimal tour with guidance.

fuel consumption can be obtained at the cost of increased mission duration.

Table 2 shows the $\Delta v$ and TOF breakdown of the fuel-optimal trajectory obtained. Figure 5 shows the plots of semi-major axis, inclination, and RAAN variations observed during the tour.

Tables 4 and 5 show the performance comparison between the three guidance schemes and the forward propagation of the PMDT outcome. The forward propagation of the phasing orbits was performed by assuming that at each time step, $\boldsymbol{f}_{\mathrm{T}} = -\eta \frac{\boldsymbol{f}_{\mathrm{d}}}{\mathrm{DC}}$. For all other legs, the out-of-plane thrust angle ($\beta$) obtained using the extended Edelbaum method was interpolated at each time step to calculate $\boldsymbol{f}_{\mathrm{T}} = \eta \frac{T_{\max}}{m} [0, \cos(\beta_{\mathrm{interp}}), \sin(\beta_{\mathrm{interp}})]$.

**Table 3** Fuel-optimal tour: Guidance coefficients obtained from PSO simulations in simplified dynamics

| Guidance | Guidance coefficient | | | | |
|---|---|---|---|---|---|
| Ruggiero | $W_a$ | $W_e$ | $W_i$ | $W_\Omega$ | |
| Leg 1 | 0.2058 | 0 | 0 | 0 | |
| Leg 2 | 0.8622 | 0 | 1 | 0 | |
| Leg 3 | 0.2058 | 0 | 0 | 0 | |
| Leg 4 | 0.8622 | 0 | 1 | 0 | |
| Leg 5 | 0.2058 | 0 | 0 | 0 | |
| $\Delta v$-law | $\lambda_{e1}$ | $\lambda_{e2}$ | $\lambda_{ai}$ | $\lambda_{ei}$ | $\lambda_{a\Omega}$ |
| Leg 1 | 0.0341 | 0.9595 | 0.7910 | 0 | 0.0006800 |
| Leg 2 | 0.1260 | 0.04625 | 0.5969 | 0.8367 | 0.01846 |
| Leg 3 | 0.0341 | 0.9595 | 0.7910 | 0 | 0.0006800 |
| Leg 4 | 0.1260 | 0.04625 | 0.5969 | 0.8367 | 0.01846 |
| Leg 5 | 0.0341 | 0.9595 | 0.7910 | 0 | 0.0006800 |
| Q-law | $W_a$ | $W_e$ | $W_i$ | $W_\Omega$ | |
| Leg 1 | 1.0 | 0 | 0.8479 | 0 | |
| Leg 2 | 0.6934 | 0 | 0.5649 | 0 | |
| Leg 3 | 1.0 | 0 | 0.8479 | 0 | |
| Leg 4 | 0.6934 | 0 | 0.5649 | 0 | |
| Leg 5 | 1.0 | 0 | 0.8479 | 0 | |

Note that it is assumed that errors that are smaller than ∼20 km in semi-major axis, ∼1 deg in RAAN, and ∼0.1 deg in inclination shall be taken care of in the proximity operation and handover phases of the mission. The coefficients of guidance were optimized using PSO such that the errors at each leg would be minimized. It can be seen that the propagation errors were reduced through the use of either guidance scheme.

Additionally, the Ruggiero guidance consumed the least fuel. The $\Delta v$-law consumed more propellant but exhibited better accuracy in tracking the semi-major axis and inclination. The Q-law consumed even more fuel but without achieving better accuracy. As Fig. 6 shows, Ruggiero guidance could track the reference RAAN through the phasing orbit in Leg 2 to a better extent than the $\Delta v$-law and Q-law.

**Table 4** Fuel-optimal tour: Error per leg obtained for each of the guidance schemes used

| Leg No. | Forward propagated PMDT | | | Ruggiero guidance | | |
|---|---|---|---|---|---|---|
| | $\Delta a$ (km) | $\Delta i$ (deg) | $\Delta\Omega$ (deg) | $\Delta a$ (km) | $\Delta i$ (deg) | $\Delta\Omega$ (deg) |
| 1 | 2.9424 | 0.000044 | 0.3086 | 0.0847 | 0.000004 | 0.1641 |
| 2 | 11.5665 | 0.050289 | 1.6496 | 0.8959 | 0.037086 | 0.1514 |
| 3 | 7.7504 | 0.000006 | 0.7289 | 1.9466 | 0.000004 | 0.1794 |
| 4 | 1.6705 | 0.023349 | 0.2748 | 0.5171 | 0.102374 | 0.1619 |
| 5 | 5.7491 | 0.000005 | 0.0060 | 5.9474 | 0.000013 | 0.3375 |
| Total | 29.6790 | 0.074 | 2.9680 | 9.3916 | 0.139 | 0.9943 |
| Leg No. | $\Delta v$-law guidance | | | Q-law guidance | | |
| | $\Delta a$ (km) | $\Delta i$ (deg) | $\Delta\Omega$ (deg) | $\Delta a$ (km) | $\Delta i$ (deg) | $\Delta\Omega$ (deg) |
| 1 | 0.1589 | 0.000068 | 0.0800 | 0.2785 | 0.000003 | 0.1470 |
| 2 | 0.3412 | 0.001 | 0.7606 | 0.2185 | 0.000745 | 0.0189 |
| 3 | 0.2365 | 0.000062 | 0.0906 | 5.8769 | 0.000003 | 0.3859 |
| 4 | 0.1256 | 0.000888 | 0.0957 | 0.0237 | 0.000631 | 0.6547 |
| 5 | 0.2256 | 0.00008 | 0.0467 | 0.0125 | 0.000023 | 0.0933 |
| Total | 1.0877 | 0.002 | 1.0736 | 6.4102 | 0.01 | 1.2998 |

**Table 5** Fuel-optimal tour: $\Delta v$, TOF, and total error comparison of guidance strategies

| Case | TOF (d) | Fuel (kg) | $\Delta a$ (km) | $\Delta i$ (deg) | $\Delta\Omega$ (deg) |
|---|---|---|---|---|---|
| Forward propagated PMDT | 1825.0 | 136.10 | 29.679 | 0.074 | 2.968 |
| Ruggiero guidance | 1825.4 | 137.11 | 9.392 | 0.139 | 0.994 |
| $\Delta v$-law guidance | 1824.6 | 138.32 | 1.088 | 0.002 | 1.074 |
| Q-law guidance | 1825.0 | 138.98 | 6.410 | 0.001 | 1.300 |

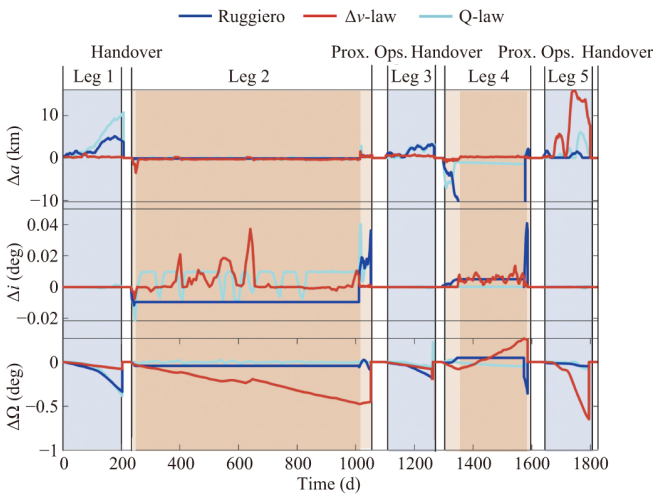


**Fig. 6** Fuel-optimal tour guidance errors present.

## 4.2 Time-optimal scenario

When generating the time-optimal result, the total $\Delta v$ was limited to less than 1500 m/s. The initial phasing orbit guess required to solve the time-optimal trajectory using fmincon was set to be the maximum of the final and initial velocities and the minimum of the final and initial inclinations. As shown in Eq. (10), higher phasing velocity and lower inclination naturally lead to a high phasing rate, reducing the time required for phasing. The first optimal phasing orbit was at $a = 7714.2$ km and $i = 99.35$ deg. The second optimal phasing orbit was at $a = 7464.5$ km and $i = 97.60$ deg. The optimization took 31.88 s to complete. The optimal TOF obtained was 1274.54 days, which occurred when $\Delta v = 1500.00$ m/s and the total fuel consumption was 166.18 kg. As this solution reached the $\Delta v$ boundary, it is evident that outcomes with better TOF can be obtained at the cost of increasing the $\Delta v$.

Table 6 shows the $\Delta v$ and TOF breakdown of the obtained time-optimal trajectory. Figure 7 shows the plots of semi-major axis, inclination, and RAAN variations observed throughout the tour. Tables 8 and 9 illustrate the variation of the guidance solutions from the forward propagated PMDT solution at various mission stages for the time-optimal case. The forward propagation had a significant RAAN and inclination error in the second leg, largely due to the low phasing orbit altitude. The Ruggiero guidance was more accurate than the $\Delta v$-law

**Table 6** Time-optimal tour: $\Delta v$ and TOF per leg

| Leg | $\Delta v$ (m/s) | TOF (d) |
|---|---|---|
| Leg 1 (from H-2A R/B to 350 km orbit) | 140.12 | 203.82 |
| Handover | — | 30.00 |
| Leg 2 (from 350 km orbit to ALOS 2) | 691.14 | 422.09 |
| Proximity operations | — | 45.00 |
| Leg 3 (from ALOS 2 to 350 km orbit) | 151.93 | 165.40 |
| Handover | — | 30.00 |
| Leg 4 (from 350 km orbit to GOSAT) | 341.67 | 141.03 |
| Proximity operations | — | 45.00 |
| Leg 5 (from GOSAT to 350 km orbit) | 175.14 | 162.20 |
| Handover | — | 30.00 |
| Total | 1500.00 | 1274.54 |

**Table 7** Time-optimal tour: Guidance coefficients obtained from PSO simulations in simplified dynamics

| Guidance | Guidance coefficient | | | | |
|---|---|---|---|---|---|
| Ruggiero | $W_a$ | $W_e$ | $W_i$ | $W_\Omega$ | |
| Leg 1 | 0.2058 | 0 | 0 | 0 | |
| Leg 2 | 0.9564 | 0 | 0.1211 | 0.00985 | |
| Leg 3 | 0.2058 | 0 | 0 | 0 | |
| Leg 4 | 0.9564 | 0 | 0.1211 | 0.00985 | |
| Leg 5 | 0.2058 | 0 | 0 | 0 | |
| $\Delta v$-law | $\lambda_{e1}$ | $\lambda_{e2}$ | $\lambda_{ai}$ | $\lambda_{ei}$ | $\lambda_{a\Omega}$ |
| Leg 1 | 0.0169 | 0.9431 | 0.9998 | 0.9010 | 0.00329 |
| Leg 2 | 0.2312 | 0.4254 | 1 | 0.1943 | 0.0724 |
| Leg 3 | 0.0169 | 0.9431 | 0.9998 | 0.9010 | 0.00329 |
| Leg 4 | 0.2312 | 0.4254 | 1 | 0.1943 | 0.0724 |
| Leg 5 | 0.0169 | 0.9431 | 0.9998 | 0.9010 | 0.00329 |
| Q-law | $W_a$ | $W_e$ | $W_i$ | $W_\Omega$ | |
| Leg 1 | 0.8784 | 0 | 0.9156 | 0.0001773 | |
| Leg 2 | 1.0 | 0 | 0.04448 | 0.009775 | |
| Leg 3 | 0.8784 | 0 | 0.9156 | 0.0001773 | |
| Leg 4 | 1.0 | 0 | 0.04448 | 0.009775 | |
| Leg 5 | 0.8784 | 0 | 0.9156 | 0.0001773 | |

guidance but consumed the highest amount of propellant. The Q-law guidance consumed the least amount of propellant and reduced the RAAN error the most. The $\Delta v$-law guidance provided a middle ground, where the inclination error was reduced at the cost of increasing the RAAN and semi-major axis errors.

The results of the time-optimal scenario reinforce the conclusion about the suitability of the PMDT for ADR mission design and of the guidance schemes in tracking the reference solutions.

## 5 Conclusions

The paper details the design and guidance of a multi-ADR mission. First, the proposed mission architecture is discussed in detail. Then, a preliminary mission design tool (PMDT) that considers the effect of drag, eclipses, duty cycle, and $J_2$ perturbations is developed to analyze the multi-ADR mission. Guidance algorithms are introduced to assess the PMDT's accuracy and to provide a method of tracking the reference trajectories. Example time and fuel optimization cases are provided for a three-debris removal mission.

The example optimizations show that the simplified models adopted in the PMDT produce good estimates of the TOF and propellant usage for a complex ADR mission. Furthermore, the three guidance schemes can track the reference trajectories with good accuracy even when osculating dynamics and realistic operational constraints are considered. Hence, the method developed

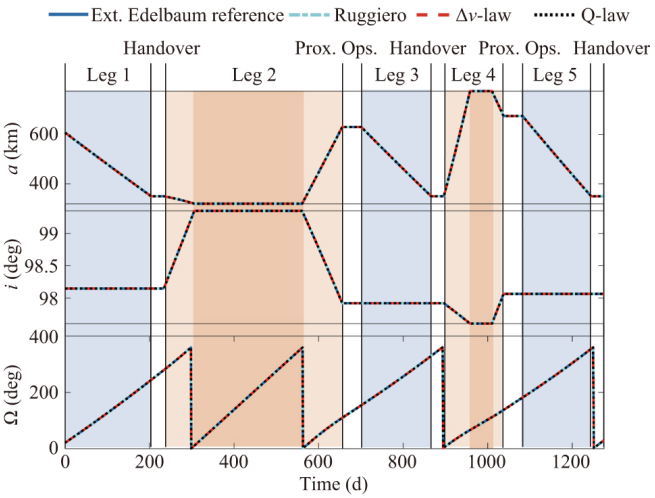


**Fig. 7** Time-optimal tour with guidance.

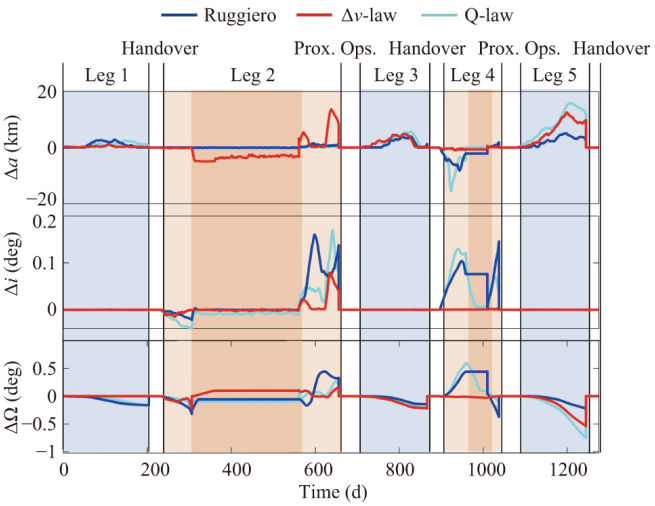


**Fig. 8** Time-optimal tour guidance errors.

**Table 8** Time-optimal tour: Error per leg obtained for each of the guidance schemes used

| Leg No. | Forward propagated PMDT | | | Ruggiero guidance | | |
|---|---|---|---|---|---|---|
| | $\Delta a$ (km) | $\Delta i$ (deg) | $\Delta\Omega$ (deg) | $\Delta a$ (km) | $\Delta i$ (deg) | $\Delta\Omega$ (deg) |
| 1 | 2.9424 | 0.000044 | 0.3086 | 0.0847 | 0.000004 | 0.1641 |
| 2 | 3.7791 | 1.315875 | 4.6885 | 0.0017 | 0.018552 | 0.2086 |
| 3 | 6.7373 | 0.000022 | 0.3806 | 1.3395 | 0.000037 | 0.1480 |
| 4 | 0.1680 | 0.016903 | 0.0190 | 0.0135 | 0.000815 | 0.0573 |
| 5 | 10.0930 | 0.000011 | 0.6387 | 2.2808 | 0.000003 | 0.2212 |
| Total | 23.7199 | 1.333 | 6.0354 | 3.7201 | 0.019 | 0.7991 |
| Leg No. | $\Delta v$-law guidance | | | Q-law guidance | | |
| | $\Delta a$ (km) | $\Delta i$ (deg) | $\Delta\Omega$ (deg) | $\Delta a$ (km) | $\Delta i$ (deg) | $\Delta\Omega$ (deg) |
| 1 | 0.1778 | 0.000107 | 0.0000 | 0.8002 | 0.000006 | 0.1672 |
| 2 | 8.4013 | 0.039387 | 0.1574 | 0.3874 | 0.084089 | 0.2247 |
| 3 | 0.1220 | 0.000006 | 0.2208 | 0.9388 | 0.000015 | 0.2020 |
| 4 | 0.1556 | 0.000676 | 0.0076 | 0.0195 | 0.002687 | 0.0007 |
| 5 | 9.7757 | 0.000067 | 0.5419 | 11.8298 | 0.000017 | 0.0755 |
| Total | 18.6324 | 0.040 | 0.9276 | 13.9756 | 0.087 | 0.6701 |

**Table 9** Time-optimal tour: $\Delta v$, TOF, and total error comparison for the guidance strategies implemented

| Case | TOF (d) | Fuel (kg) | $\Delta a$ (km) | $\Delta i$ (deg) | $\Delta\Omega$ (deg) |
|---|---|---|---|---|---|
| Forward propagated PMDT | 1274.5 | 166.18 | 23.720 | 1.333 | 6.035 |
| Ruggiero guidance | 1274.4 | 168.87 | 3.720 | 0.019 | 0.799 |
| $\Delta v$-law guidance | 1274.2 | 167.67 | 18.632 | 0.040 | 0.928 |
| Q-law guidance | 1274.6 | 167.10 | 13.976 | 0.087 | 0.670 |

can optimize multi-ADR missions with a good degree of accuracy and limited computational cost. The guidance laws can track the reference trajectories computed by the PMDT to effectively exploit the $J_2$ perturbation to reduce the propellant cost associated with making RAAN changes. The PMDT performance is expected to degrade with the inclusion of additional perturbations and errors, such as thrust execution and orbit determination. However, the guidance laws could provide similar accuracy in higher fidelity dynamics due to the feedback mechanisms present. Simulations performed with high-fidelity dynamics are beyond the scope of this work and shall be explored in the future.

## Acknowledgements

This project was partially supported by the Ministry of Business, Innovation and Employment (MBIE) study: Astroscale/ Rocket Lab/ Te Pūnaha Ātea-Space Institute Active Debris Removal Study.

## Funding note

Open Access funding enabled and organized by CAUL and its Member Institutions.

## Declaration of competing interest

The authors have no competing interests to declare that are relevant to the content of this article.

## References

[1] Maestrini, M., Di Lizia, P. Guidance strategy for autonomous inspection of unknown non-cooperative resident space objects. *Journal of Guidance, Control, and Dynamics*, **2022**, 45(6): 1126–1136.

[2] Kessler, D. J., Cour-Palais, B. G. Collision frequency of artificial satellites: The creation of a debris belt. *Journal of Geophysical Research*, **1978**, 83(A6): 2637–2646.

[3] Kessler, D. J., Johnson, N. L., Liou, J.-C., Matney, M. The Kessler syndrome: Implications to future space operations. In: Proceedings of the Advances in the Astronautical Sciences, **2010**: AAS 10-016.

[4] Pelton, J. N. *Space Debris and Other Threats from Outer Space*. New York: Springer, **2013**.

[5] Mark, C. P., Kamath, S. Review of active space debris removal methods. *Space Policy*, **2019**, 47: 194–206.

[6] Potter, S. NASA administrator statement on Russian ASAT test. **2021**. Available at https://www.nasa.gov/press-release/nasa-administrator-statement-on-russian-asat-test.

[7] Bonnal, C., Ruault, J. M., Desjean, M. C. Active debris removal: Recent progress and current trends. *Acta Astronautica*, **2013**, 85: 51–60.

[8] Liou, J. C. An active debris removal parametric study for LEO environment remediation. *Advances in Space Research*, **2011**, 47(11): 1865–1876.

[9] Forshaw, J. L., Aglietti, G. S., Fellowes, S., Salmon, T., Retat, I., Hall, A., Chabot, T., Pisseloup, A., Tye, D., Bernal, C., *et al.* The active space debris removal mission RemoveDebris. Part 1: From concept to launch. *Acta Astronautica*, **2020**, 168: 293–309.

[10] White, A. E., Lewis, H. G. The many futures of active debris removal. *Acta Astronautica*, **2014**, 95: 189–197.

[11] Cerf, M. Fast solution of minimum-time low-thrust transfer with eclipses. *Proceedings of the Institution of Mechanical Engineers, Part G: Journal of Aerospace Engineering*, **2019**, 233(7): 2699–2714.

[12] Rimani, J., Paissoni, C. A., Viola, N., Saccoccia, G., Gonzalez del Amo, J. Multidisciplinary mission and system design tool for a reusable electric propulsion space tug. *Acta Astronautica*, **2020**, 175: 387–395.

[13] Viavattene, G., Devereux, E., Snelling, D., Payne, N., Wokes, S., Ceriotti, M. Design of multiple space debris removal missions using machine learning. *Acta Astronautica*, **2022**, 193: 277–286.

[14] Ruggiero, A.; Pergola, P.; Marcuccio, S.; Andrenucci, M. Low-thrust maneuvers for the efficient correction of orbital elements. In: Proceedings of the 32nd International Electric Propulsion Conference, **2011**: IEPC-2011-102.

[15] Locoche, S. An analytical method for evaluation of low-thrust multi-revolutions orbit transfer with perturbations and power constraint. In: Proceedings of the Conference on Guidance, Navigation and Control Systems, **2018**: 10–20.

[16] Petropoulos, A. E. Refinements to the Q-law for the low-thrust orbit transfers. In: Proceedings of the 15th AAS/AIAA Space Flight Mechanics Conference, **2005**: AAS 05-162.

[17] Astroscale TA Rocket Lab. Active debris removal feasibility study final report. **2021**.

[18] Jones, H. Estimating the life cycle cost of space systems. In: Proceedings of the 45th International Conference on Environmental Systems, **2015**: ICES-2015-041.

[19] Edelbaum, T. N. Propulsion requirements for controllable satellites. *ARS Journal*, **1961**, 31(8): 1079–1089.

[20] Colasurdo, G., Casalino, L. Optimal low-thrust maneuvers in presence of Earth shadow. In: Proceedings of the AIAA/AAS Astrodynamics Specialist Conference and Exhibit, **2004**: AIAA 2004-5087.

[21] Kechichian, J. A. Reformulation of Edelbaum's low-thrust transfer problem using optimal control theory. *Journal of Guidance, Control, and Dynamics*, **1997**, 20(5): 988–994.

[22] Kluever, C. A. Using Edelbaum's method to compute low-thrust transfers with Earth-shadow eclipses. *Journal of Guidance, Control, and Dynamics*, **2011**, 34(1): 300–303.

[23] Neta, B., Vallado, D. On satellite umbra/penumbra entry and exit positions. *The Journal of the Astronautical Sciences*, **1998**, 46(1): 91–103.

[24] Cerf, M. Optimal plan for multiple debris removal missions. *RAIRO - Operations Research*, **2017**, 51(4): 1005–1032.

[25] Gondelach, D. J., Armellin, R. Element sets for high-order Poincaré mapping of perturbed Keplerian motion. *Celestial Mechanics and Dynamical Astronomy*, **2018**, 130(10): 65.

**Minduli C. Wijayatunga** received her B.Sc. and B.Eng degrees in aerospace engineering, physics, and mathematics from the University of Sydney, Australia, in 2020. She is pursuing a Ph.D. at the Te Pūnaha Ātea Space Institute in the University of Auckland, New Zealand. Her research interests include trajectory design, proximity operations, and space debris removal. E-mail: mwij516@aucklanduni.ac.nz

**Roberto Armellin** received his M.Sc. and Ph.D. degrees in aerospace engineering from Politecnico di Milano, Italy, in 2003 and 2007, respectively. Since November 2020, he has been a professor at Te Pūnaha Ātea - Space Institute at the University of Auckland, New Zealand. His current research interests include space trajectory optimization, spacecraft navigation and guidance, and space situational awareness. E-mail: roberto.armellin@auckland.ac.nz

**Harry Holt** received his M.Sc. degree in natural sciences (physics) from the University of Cambridge, UK, in 2018. He completed his Ph.D. at the University of Surrey, UK, in 2022, working on trajectory design using Lyapunov control laws and reinforcement learning. He is now working as a research fellow at Te Pūnaha Ātea - Space Institute, at the University of Auckland, New Zealand. His research interests include trajectory design, Lyapunov control, and reinforcement learning. E-mail: harry.holt@auckland.ac.nz

**Laura Pirovano** received her M.Sc. degree in aerospace engineering (space exploration track) from TU Delft, the Netherlands, in 2015. She completed her Ph.D. at the University of Surrey, UK, in 2020, on methods for cataloging space debris with optical observations. She is now a research fellow at Te Pūnaha Ātea - Space Institute, at the University of Auckland, New Zealand. Her research interests include space situational awareness and uncertainty propagation. E-mail: laura.pirovano@auckland.ac.nz

**Aleksander A. Lidtke** graduated from the University of Southampton, UK, with an M.Eng. degree in aerospace engineering in 2013. He then obtained his Ph.D. degree in the field of space debris in 2016, also from the University of Southampton. He then proceeded to work in the industry as a lead systems and lead satellite test engineer for several years. He currently works at Astroscale Japan, bringing all this experience together with the aim of improving the sustainability of spaceflight by deploying active debris removal missions. His research interests include spacecraft guidance, navigation and control, space surveillance and tracking, and model-based systems engineering. E-mail: a.lidtke@astroscale.com